Molecular Dynamics Investigation of the ω-Current in the Kv1.2 Voltage Sensor Domains

Fatemeh Khalili-Araghi,[†§] Emad Tajkhorshid,[‡] Benoît Roux,[§] and Klaus Schulten[†*]
[†]Department of Physics and [‡]Department of Biochemistry, University of Illinois at Urbana-Champaign, Urbana, Illinois; and [§]Department of Biochemistry and Molecular Biology, University of Chicago, Chicago, Illinois

ABSTRACT   Voltage sensor domains (VSD) are transmembrane proteins that respond to changes in membrane voltage and modulate the activity of ion channels, enzymes, or in the case of proton channels allow permeation of protons across the cell membrane. VSDs consist of four transmembrane segments, S1–S4, forming an antiparallel helical bundle. The S4 segment contains several positively charged residues, mainly arginines, located at every third position along the helix. In the voltage-gated *Shaker* K$^+$ channel, the mutation of the first arginine of S4 to a smaller uncharged amino acid allows permeation of cations through the VSD. These currents, known as ω-currents, pass through the VSD and are distinct from K$^+$ currents passing through the main ion conduction pore. Here we report molecular dynamics simulations of the ω-current in the resting-state conformation for Kv1.2 and for four of its mutants. The four tested mutants exhibit various degrees of conductivity for K$^+$ and Cl$^-$ ions, with a slight selectivity for K$^+$ over Cl$^-$. Analysis of the ion permeation pathway, in the case of a highly conductive mutant, reveals a negatively charged constriction region near the center of the membrane that might act as a selectivity filter to prevent permeation of anions through the pore. The residues R1 in S4 and E1 in S2 are located at the narrowest region of the ω-pore for the resting state conformation of the VSD, in agreement with experiments showing that the largest increase in current is produced by the double mutation E1D and R1S.

INTRODUCTION

Voltage-gated potassium (Kv) channels are membrane proteins that respond to changes in transmembrane potential, and allow passage of K$^+$ ions across the cell membrane. The ion conduction pore is located in the middle of a tetrameric structure, surrounded by four voltage sensor domains (VSD). Upon changes in transmembrane potential, the VSDs go from a resting to an active state conformation, which causes the opening of the central ion conduction pore. Crystallographic x-ray structures are available for the active state conformation (1–3), but there is currently no atomic-resolution structure of a Kv channel in the resting state. Information about the conformation of the VSD in the resting state has been gained indirectly from a wide range of experiments.

The available crystal structures show that the VSD consists of four transmembrane helices (S1–S4), which form an antiparallel four-helical bundle at the periphery of the channel within the lipid membrane. The fourth transmembrane segment (S4) contains several positively charged residues (R1, R2, R3, R4, K5, and R6), located at every third position of the amino acid sequence of the protein. These charged residues move within the transmembrane electrostatic field and drive the opening of the channel (4–8). The discovery of a voltage-gated phosphatase (Ci-VSP) (9) and a voltage-gated proton channel (Hv) (10,11), possessing a domain with high sequence similarity to S1–S4, suggest that the VSD is an independent functional module.

Knowledge of the activated and resting conformational states is necessary to understand the voltage-gating of K$^+$ channels at the atomic level. Lack of an atomic-resolution structure for the resting state of the VSD motivated efforts aimed at translating the results from various experiments into structural information using computational modeling (7,12–20). One class of particularly intriguing experiments concerns mutations causing state-dependent ion conduction through the VSD module itself. Although ions do not flow through the wild-type VSD of K$^+$ channels under standard conditions, it has been shown that substitution of R1 by a histidine residue gives rise to a proton pore through the VSD of the *Shaker* K$^+$ channel at hyperpolarized potentials (21,22). Interestingly, this result preceded the discovery of the voltage-gated proton channel Hv (10,11). It was also shown that mutation of the first gating arginine (R1) to a smaller uncharged amino acid in the *Shaker* K$^+$ channel makes the VSD permeable to ions (15,23,24); such currents, now called ω-currents, can be observed when the central ion conduction pore is nonconducting. Analysis showed that the ions pass through an aqueous crevice, the so-called ω-pore, which is formed within each VSD (15). The ω-pores display some specificity for monovalent cations, with a weak preference for larger ions like Cs$^+$ (23). Substitution of Cl$^-$ ions with large organic anions in the solution does not alter the magnitude of the current, indicating that the current is not predominantly carried by anions (23). The current can also be carried by the large guanidinium ions, which has led to the conclusion that the ionic pathway, at least partially, is the same pathway as that experienced by the gating arginines within the VSD (23).

In the absence of an atomic-resolution structure for the resting state conformation of the VSD, the conduction pathway and the nature of ion selectivity in the ω-pore remain elusive. Mutational studies have identified and characterized residues of the VSD, for which manipulation of the residue side chains affects the magnitude of the ω-current in the *Shaker* K$^+$ channel (15). Presumably, the residues identified experimentally as part of the ω-pore interact with permeating ions, either electrostatically or sterically. However, because the location of key residues is not uniquely defined with respect to the ω-pore, such results cannot readily be translated into a structural model for the resting state of the VSD. It is possible, nonetheless, to test whether a proposed structural model of the VSD is, or is not, consistent with experimental observations. In a previous study, Delemotte et al. (18) simulated the state-dependent ω-currents through the VSD of the Kv1.2 channel. The study showed that an outward ω-current could be observed through the activated state conformation of the Kv1.2 channel (based on the x-ray structure) for the K5 and R6 mutants. This result gives us confidence that one can use ω-currents to assess the validity of a conformational model of the VSD in the resting state.

In the present study, we examine ion permeation through the ω-pore of a resting state model of the VSD for several of its mutants. There are two main motivations for returning to the problem of ion permeation through the ω-pore given the previous study by Delemotte et al. (18). First, the present study is focused on several single and double mutations supporting the occurrence of the ω-current at hyperpolarizing potential when the VSD is in its resting state. In contrast, Delemotte et al. (18) simulated both the activated and resting state of the channel, but considered only a single mutant for the latter (R1); double mutants, in particular, provide critically important information about the resting state conformation of the VSD (15). Second, the two studies are based on distinct models of the resting state conformation of the VSD that were generated with two very different strategies. The conformation of the VSD used here is taken from a complete structural model of the Kv1.2 channel in its resting state that was initially constructed using the Rosetta Membrane prediction program (13) and then subsequently refined using all-atom molecular dynamics simulations (20). This model proved stable in long MD simulations in the presence of a membrane voltage, and the calculated gating charge (relative to the open state models obtained based on the crystallographic structure of Kv1.2) corresponds to 13 unit charges, in agreement with experimental data (25–27). In contrast, the resting state model of Delemotte et al. (18) was generated by imposing a set of distance restraints deduced from some experimental data. Despite broad similarities, the position of the S4 helix and the orientation of the side chain of arginine R1 relative to the S2 helix are different in the two models. Comparison with the experimental results on single and double mutants of the *Shaker*

K$^+$ channel broadly support our structural model of the resting-state conformation of the VSD (15).

METHODS

Simulation setup

The simulated wild-type system consists of the VSD (residues 161–325) of the Kv1.2 potassium channel embedded in a patch of DPPC lipid bilayer surrounded by an aqueous solution of 100 mM KCl. The initial coordinates of the protein (VSD) in the resting state were taken from the atomic models of the VSD presented in Khalili-Araghi et al. (20). The procedure of constructing the protein/membrane system is the same as the one described for simulations of individual VSDs in Khalili-Araghi et al. (20).

The system was equilibrated for 10 ns in the following multistage protocol. After 5000 steps of minimization with all protein atoms constrained, the hydrocarbon tails of the lipid molecules were allowed to relax for 500 ps. The system was then equilibrated for 1 ns with the protein backbone restrained, followed by 8.5 ns of free equilibration at a voltage bias of −250 mV. The negative voltage bias across the membrane stabilizes the resting state of the VSD. During all the simulations, the backbone atoms of the S4-S5 linker (residues 312–325) were constrained harmonically to their initial position. The simulations were performed in an NP_nAT ensemble (P_n = 1 atm, T = 318 K), in which the cross-sectional area of the lipid bilayer (A) is kept constant after the initial adjustment.

Mutants setup and simulations

Critical basic and acidic residues of the wild-type VSD in the Kv1.2 channel are: R294 (R1), R297 (R2), R300 (R3), R303 (R4), K306 (K5), R309 (R6) along S4, E183 (E0) along S1, E226 (E1) and E236 (E2) along S2, and D259 (D3) along S3. In addition to the wild-type VSD, four additional systems were simulated in which R1 was mutated to a serine or an asparagine. In two of these mutants, E1 on S2 was also mutated to an aspartic acid.

The equilibrated configuration of the resting state VSD (20), obtained from the 10-ns equilibration, was used to prepare each of the four mutant systems. Using the program VMD (28), the atomic coordinates of the residues to be mutated were replaced by those of the mutant based on the internal coordinates of each amino acid side chain in the CHARMM27 force field (29,30). Water molecules clashing with the new residues were removed and the systems were neutralized by randomly removing an ion carrying the extra charge. Each of the four mutants was then equilibrated in a hydrated DPPC lipid bilayer for 10 ns, at a voltage bias of −250 mV.

The final configurations obtained from equilibration simulations of the VSD and the four mutants were further simulated to monitor the ω-currents passing through the VSD. These simulations were carried out at a voltage bias of −750 mV for 100 ns or at a voltage of −1 V for 50 ns. The average root mean-squared deviation of the protein backbone during these simulations varied in the range of 2.6–3.6 Å relative to the initial conformation of the VSD (see Table S1 in the Supporting Material), indicating that the VSD retained its resting state conformation during the simulations.

The simulations were repeated at a voltage bias of −500 mV as the conductivity of the ω-pore (~0.3 pS (15)) proved to be too low to observe the permeation of ions within the timescale of the simulation except for very negative membrane potentials. Ion permeation in K$^+$ channels has been simulated at comparable membrane potentials (31,32). In such simulations, the short timescale of the simulations (compared to biologically relevant timescales) prevents adverse effects of the high potentials applied.

RESULTS AND DISCUSSION

To characterize the conduction pathway and ionic selectivity of the ω-pore, we carried out MD simulations of the

VSD (from Kv1.2) and four of its mutants in a membrane/ solvent environment. In the *Shaker* K$^+$ channel, mutation of the first gating arginine (R1) to a smaller uncharged residue is necessary to obtain conductive channels (23). Additional mutation of a conserved glutamic acid on S2, corresponding to E226 (E1) in Kv1.2, to smaller residues such as aspartic acid increases the observed currents significantly (15). Specifically, we have simulated the single mutants of VSD, R1S and R1N, as well as the double mutants E1D-R1S and E1D-R1N, for which an enhanced conductivity through the ω-pore is expected; the second mutation (E1D) is known to increase the magnitude of the current in the R1S mutant by a factor of 4–6 (15). The stated mutations are expected to involve only a small perturbation to the original system. Snapshots of the VSD in its resting state and the mutation site in each of the four mutants are shown in Fig. 1. In the following, quantitative agreement with measured ω-currents cannot be expected, even when simulations are based on accurate atomic resolution structures of a pore; ion permeation properties are not quantitatively reproduced (33). We note in this regard that a difference in free energy barrier as small as 1.3 kcal/mol results in a 10-fold increase in the simulated current.

An ion conduction pore inside VSD

To investigate the relative conductivity of the four mutants, R1N, R1S, E1D-R1N, and E1D-R1S, each mutant system was simulated in the presence of an electric field corresponding to a hyperpolarizing membrane potential (-750 mV or -1 V). At -750 mV, the wild-type channel remains sealed, allowing passage of only one Cl$^-$ ion within 100 ns. At the higher voltage bias of -1 V, the wild-type channel breaks down, resulting in both K$^+$ and Cl$^-$ ions to rush into a wide, water-filled pore formed at this voltage within the VSD. The four mutants tested remain intact during all simulations, exhibiting various conductivities for both K$^+$ and Cl$^-$ ions. K$^+$ ions flow from the extracellular side of the channel toward the intracellular side, whereas Cl$^-$ ions traverse the channel in the opposite direction.

Table 1 shows the total number of K$^+$ and Cl$^-$ ions that cross the membrane during simulation of the four mutants. At the lower voltage bias of -750 mV, the single mutants, R1N and R1S, do not conduct any ions within 100 ns. At -1 V, these mutant channels allow passage of four and three ions, respectively, within the first 50 ns of simulation. Mutation of E1 to D, in the case of the double mutants, E1D-R1N and E1D-R1S, increases the conductivity. The highly conductive mutant, E1D-R1S, allows passage of 28 ions (18 K$^+$ and 10 Cl$^-$ ions) within 100 ns at -750 mV, and 32 ions (23 K$^+$ and 9 Cl$^-$ ions) within 50 ns at -1 V. The ionic trajectories are shown in Figs. 2 and 3.

The higher conductance rate of the double mutants is consistent with the electrophysiological experiments of Tombola et al. (15) in which mutation of E1 to D increases the ω-current in the *Shaker* K$^+$ channel. The mutation of the glutamic acid E1 to a smaller side chain (aspartic acid) breaks the salt bridge between R1 and E1 (which seals the ω-pore in the wild-type channel) and widens the pore, resulting in a more conductive channel. Whereas the two single mutants R1N and R1S show only very small conductivities in the simulations, the double mutants E1D-R1N and E1D-R1S exhibit a higher conductance, with the E1D-R1S mutant forming the most conductive ω-pore in the simulations.

Permeation of an ion through the ω-pore is a stochastic event. Conduction of ions through the pore is followed by silent intervals, in which no permeation events are observed, followed again by ion conduction. For example, the highly
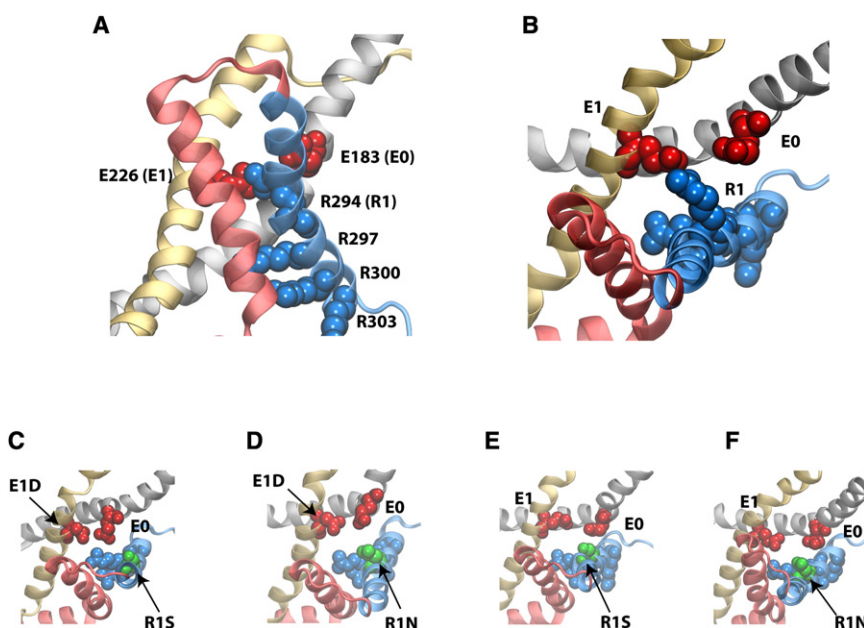

FIGURE 1 Voltage sensor domain. (*A*) (*Cartoon representation*) The voltage sensor domain of Kv1.2 in the resting state (20) (S1–S4 helical segments are colored in *yellow*, *red*, and *blue*, respectively). (*van der Waals representation*) Gating arginines, R294 (R1), R297, R300, and R303, as well as two acidic residues E226 (E1) and E183 (E0). A detailed view of the mutation site, including residues E1 and R1, is shown in panel *B* from a view perpendicular to that in panel *A*. (*C–F*) Close-up views of the mutation site in each of the four mutants, taken from a snapshot after 10 ns of equilibration.

TABLE 1   Number of ions passing through the ω-pore in the simulations

Simulated VSD	−0.75 V, 100 ns (K⁺,Cl⁻)	−1 V, 50 ns (K⁺,Cl⁻)
Wild-type	(0,1)	(27,33)*
R1N	(0,0)	(2,2)
R1S	(0,0)	(2,1)
E1D-R1N	(1,0)	(6,2)
E1D-R1S	(18,10)	(23,9)

*Wild-type VSD breaks apart during the simulation at −1 V, allowing water molecules to rush into a wide pore formed within the VSD.

conductive mutant, E1D-R1S, remains silent for 40 ns at a time, at −750 mV. The stochastic nature of the permeation does not allow one to determine accurately the pore conductivity, in particular, in the case of the single mutants with the lowest conductivity. However, the highly conducting double mutants, in particular E1D-R1S, exhibit simulated conductances that are in very good agreement with the experiments of Tombola et al. (15). Simulations of the ω-current through single mutant VSDs by Delemotte et al. (18) have shown currents of similar magnitude in Kv1.2.

Analysis of the pore radius profile along the z axis, normal to the membrane plane, shows that the narrowest region in the wild-type channel involves the salt bridge interaction between R1 and E1, which effectively blocks the pore by reducing its radius to <1 Å. Mutation of the arginine (R1) to either asparagine or serine increases the narrowest pore radius to ~1.5 Å. Mutation of the conserved glutamic acid, E1, to the shorter aspartic acid (D) widens the pore from the intracellular side and reduces the length of the narrow

constriction at the position of R1. The pore radius profile in the wild-type channel and for each of the four mutants is compared in Fig. S1 in the Supporting Material. There is a slight increase in the radius of the pore in the mutants compared to the wild-type VSD. This result bears some similarities to the observations made previously by Delemotte et al. (18), although there are also some differences. These authors described the formation of ω-pores in mutant VSDs as a "swollen-stable structure in which a connected hydrated pathway opened up between the intra- and extracellular media." Although formation of a connected hydrated pathway through the VSD is also seen in our simulations, the overall configuration of the backbone appears to be largely unchanged compared to the wild-type (see Table S1). In particular, no significant swelling of the VSD driven by the penetration of water molecules is observed in the current simulations. The root mean-squared deviation of residues E1D and R1S relative to their equilibrium conformation in the highly conducting mutant E1D-R1S is ~1.7 Å, indicating relative stability of the protein during the −1 V and −750 mV simulations. Widening of the pore is mainly due to side-chain modifications, in which R1 and E1 residues are replaced with smaller side-chain amino acids such as serine, asparagine, or aspartic acid. Increased hydration of the E1D-R1S mutant, as seen in water density profiles within the VSD (see Fig. S2), in fact, is due to high polarity of the smaller side chains rather than a swelling of the VSD.

The different behavior observed in the two simulation studies may be due to the differences in the conformational model of the resting state of the VSD. However, there
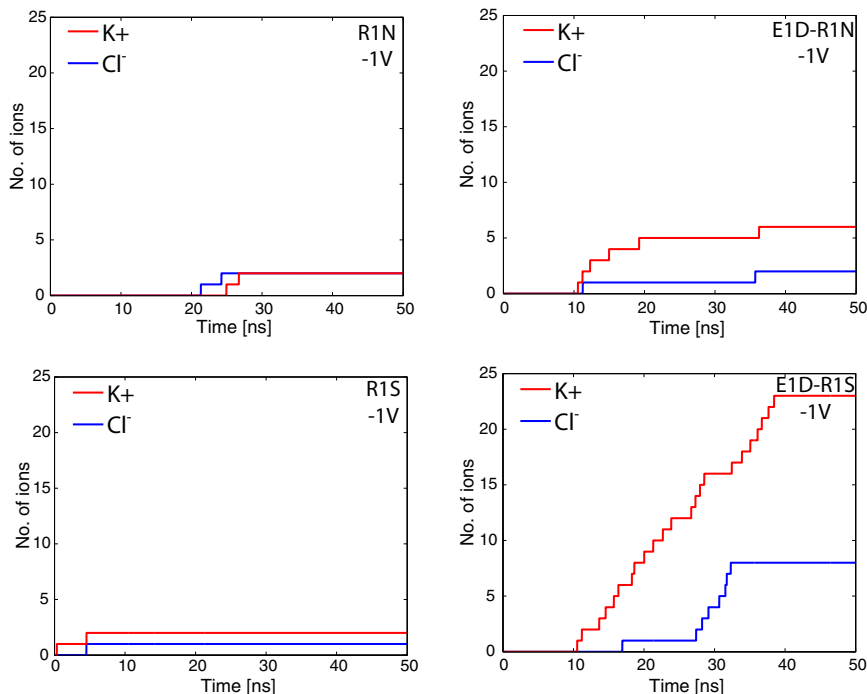

FIGURE 2   Number of K⁺ and Cl⁻ ions passing through the ω-pore in each of the four Kv1.2 mutants simulated at a hyperpolarizing membrane potential of −1 V.
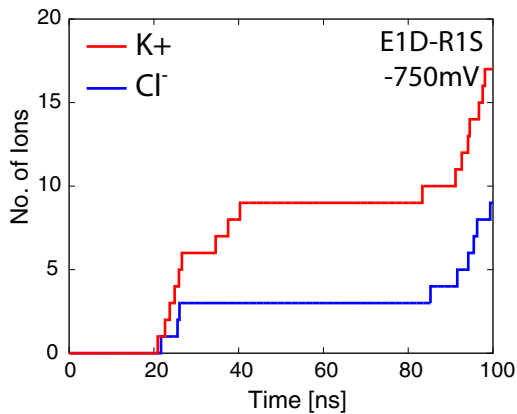
FIGURE 3   Number of K$^+$ and Cl$^-$ ions passing through the ω-pore in the highly conducting mutant of Kv1.2, E1D-R1S, simulated at -750 mV.

are also differences in the way that the mutations were represented in the simulations studies. For example, the mutations R1N or R1S were modeled explicitly in this study, whereas amino acid substitutions at R1 were approximated via an artificial uncharged isoster of arginine in the simulations of Delemotte et al. (18).

Twisted permeation pathway

Fig. 4 shows the permeation pathway of a single K$^+$ or Cl$^-$ ion within the ω-pore of the highly conductive mutant E1D-R1S. K$^+$ ions enter the VSD from the extracellular side, sliding along the S1 and S2 helices before crossing the (negatively charged) constriction region near $z = 5$ Å. After crossing the narrow barrier, K$^+$ ions exit the channel quickly (i.e., within picoseconds) in the middle of the VSD. The presence of a highly focused electric field across the intracellular half of the VSD (20,34) facilitates quick passage of the ions through the pore. Calculation of the electrostatic potential within the VSD of Kv1.2 has shown that the transmembrane potential gradient arises between $z = 5$ Å and $z = -5$ Å within the internal cavities of the VSD (20), resulting in a strong electrostatic driving force acting on the permeant ions.

Cl$^-$ ions enter the channel from the intracellular solution, slide along the S4 segment, and pass through the narrow barrier within a few picoseconds of the simulation. During their exit toward the extracellular solution, Cl$^-$ ions flow along the S3-S4 paddle with minor contacts with S1 and S2 helices. In the full-length tetrameric channel (Kv1.2), the VSDs lean on the tetrameric pore and the S3-S4 segments make contact with the pore domain. The resulting interactions are suggested to have functional impact on the voltage-gating of the full-length channel (35–37). Electrophysiological measurements of the ω-current in the *Shaker* potassium channel also included the main conduction pore (α-pore) and identified several residues on the TM helices of the pore domain that interact significantly with the permeant ion (sterically or electrostatically). The trajectories of K$^+$ and Cl$^-$ ions, presented in Fig. 4, indicate that the inclusion of the pore domain in the experiments could affect the ω-current pathway of the ions near the extracellular side of the VSD, as the ions enter or exit the ω-pore between helices S1 and S4. Nevertheless, the main characteristics of the ω-current, e.g., the actual conduction pathway and the nature of its selectivity, should be realistically described by our VSD-only simulations.

To further characterize the permeation pathway of ions within the ω-pore, the trajectories of the K$^+$ and Cl$^-$ ions are mapped onto the three-dimensional structure of the protein. Fig. 5 highlights the transmembrane residues of the VSD that interact closely with the permeant ions for the highly conductive mutant E1D-R1S. The average time that each permeant ion spends within 3 Å of particular side chains was calculated for each of the four transmembrane segments (S1–S4). The contact time of residues that are within 3 Å of permeating ions for at least 50 ps is shown in Fig. 5; the residue positions are highlighted in Fig. 6. Negatively charged residues localized on the extracellular side of the VSD ($z > 0$) interact closely with the K$^+$ ions as the latter enter the vestibule. A cluster of aspartic and glutamic acids (D190, E191, E193, and D194) located at the extracellular mouth of the VSD (on S1) provides an attractive well for positively charged K$^+$ ions. Farther down the
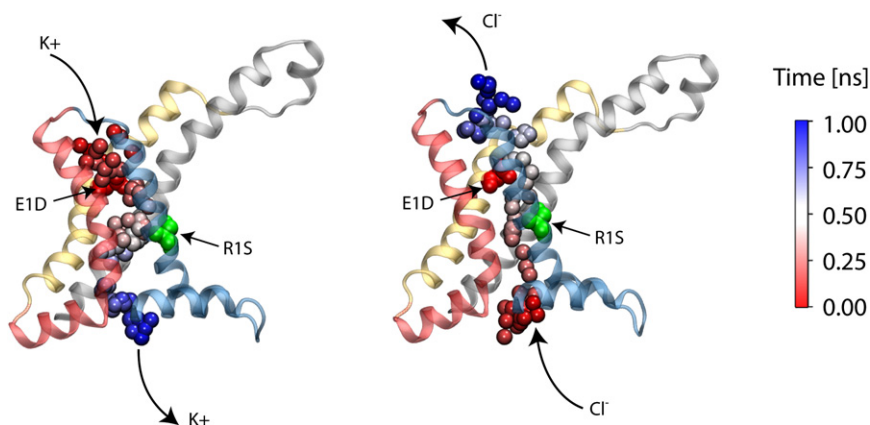

FIGURE 4   Permeation pathway of a single K$^+$ or Cl$^-$ ion within the ω-pore of Kv1.2, E1D-R1S, at -750 mV. The VSD (*cartoon representation*), with the mutated sites, E1D and R1S, highlighted (*van der Waals representation*). (The permeant ion's trajectory, ion shown as sphere, is colored from *red* to *white* to *blue* showing the time evolution of the ion position within the 1 ns segment of trajectory displaying the single conduction event.)
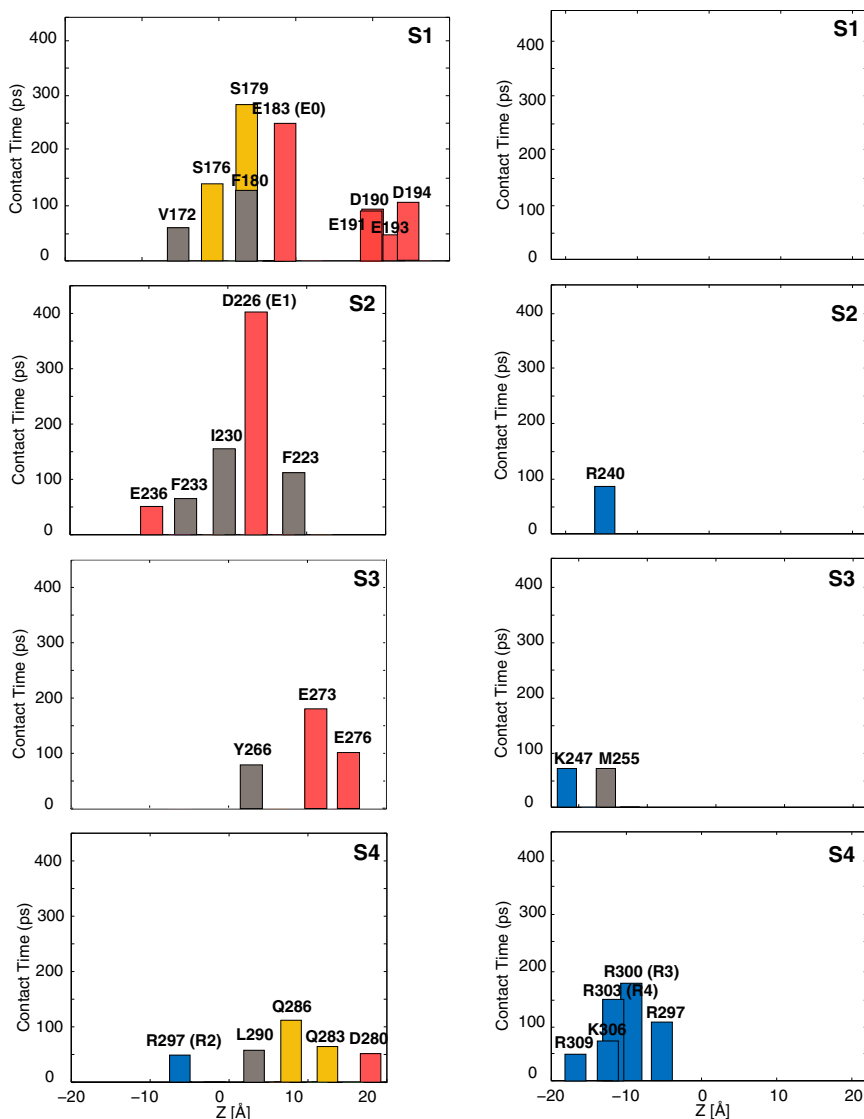
FIGURE 5 Average time that the permeant ions, K^+ (*left*) and Cl^- (*right*), spent within 3 Å of a residue side chain for the high-conducting mutant E1D-R1S, during the 100-ns simulation at −750 mV. For clarity, only residues that are within 3 Å of permeating ions for at least 50 ps are shown. (The acidic, basic, hydrophobic, and hydrophilic residues are colored in *red*, *blue*, *gray*, and *yellow*, respectively.) The *z* value shown on the horizontal axis corresponds to the average position of the residue backbone along the membrane normal.

vestibule, the pathway for K^+ ions is lined with residues E0, E1, and E273 from the S1, S2, and S3 segments, respectively. Localization of the negatively charged residues near the extracellular side of the vestibule facilitates the entrance of K^+ ions into the pore.

In the middle of the VSD ($1 \text{ Å} < z < 6 \text{ Å}$), the ω-pore is lined by four residues, E0, E1D, Y266, and L290 from the S1, S2, S3, and S4 segments, respectively. These residues form a narrow constriction in the pore that does not exceed 3 Å in radius for any of the four mutants (see Fig. S1). However, the pore is still wide enough at the constriction to allow passage of a single K^+ through the pore. The constriction region of the ω-pore and the residues lining the conduction pathway are highlighted in Fig. 7.

Cl^- ions enter the channel from the intracellular side and move along the S4 segment toward the narrow region of the vestibule. Positively charged residues on S2 (R240), S3 (K247), and S4 (R297, R300, R303, K306, and R309)

interact closely with the Cl^- ion as it moves toward the extracellular side (Fig. 5). No specific interactions between the Cl^- ions and the extracellular side of the ω-pore are observed in the simulation trajectories. The transmembrane potential gradient, focused within the intracellular crevice of the VSD, facilitates passage of Cl^- ions along the positively charged residues localized on the intracellular half of the VSD.

Channel-forming residues

The simulations of ion conduction through the VSD permit one to identify the amino acids that form the ω-pore and make direct contact with the permeant ions. Most prominent in this respect are the side groups forming a constriction region near the center of the VSD. The constriction region is formed by E0, E1D, Y266, and L290. E0 and E1D correspond to the highly conserved residues E247 and E283 in
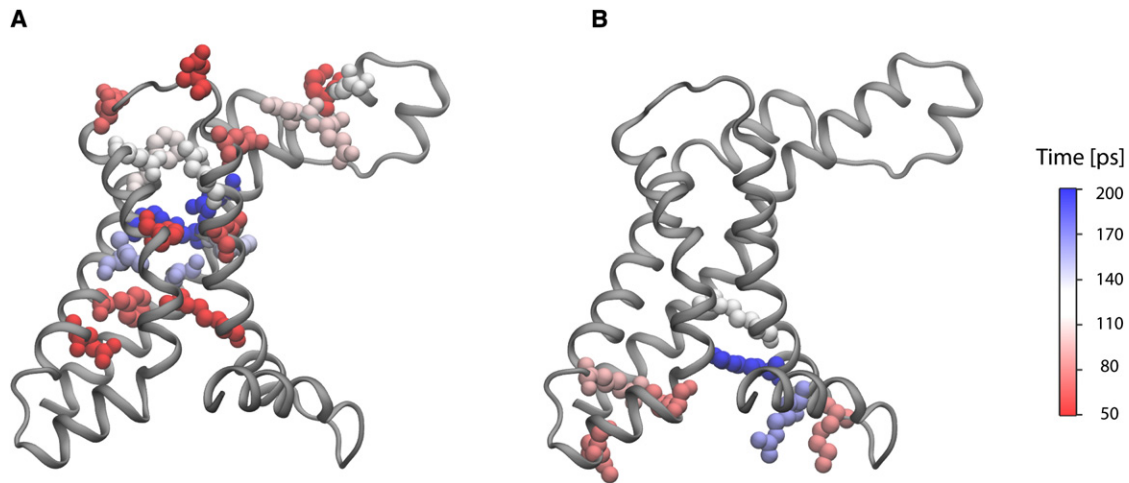
FIGURE 6 Residues making significant contact with the permeating (*A*) K$^+$ and (*B*) Cl$^-$ ions. (*Cartoon representation*) The protein backbone. (*Licorice representation*) The residues shown in Fig. 5 are highlighted, and colored according to the total time spent near permeating ions.

the *Shaker* K$^+$ channel and their role in salt-bridge interactions between VSD helices has been described previously (18,20,38,39). Two serine residues, S176 and S179, are located below the constriction region on the S1 segment. Through their close interaction with the incoming K$^+$ ion, these two polar residues attract the ions toward the S1 segment, and away from the gating arginines. Three phenylalanine residues, F180, F223, and F233, located above and below the constriction region, interact closely with the permeant ions, as does a glutamine Q286 of the S4 helix.

In a recent study, Tombola et al. (15) have characterized the effect of mutations of the VSD residues on the magnitude of the ω-current in the *Shaker* K$^+$ channel. Each residue was modified by attaching bulky, positively or negatively charged reagent molecules to cysteine mutants. The ω-currents were found to be affected by either short-range steric interactions or through long-range electrostatics, but

not necessarily through direct contact. Table 2 compares the positions identified in our simulation as interacting through direct contact (i.e., within 3 Å) with the permeating ions and the corresponding high-impact positions identified in experiment (15).

The simulations identify 18 residues within the transmembrane region of the VSD (-20 Å $< z < 20$ Å) that interact closely with the permeating K$^+$ ions. These residues include the 10 high-impact residues identified by Tombola et al. (15), as shown in Table 2. Six other residues, including S179 (on S1), I230 and E236 (on S2), Y266 (on S3), and D280 and Q283 (on S4) had not been tested in the experiments and are identified here for the first time, to our knowledge, as residues lining the permeation pathway of the ω-pore. E273 and E276 (on S3) correspond to V330 and E333 in the *Shaker* K$^+$ channel, the mutation of which does not change the magnitude of the ω-current significantly, but are shown to interact closely with the permeant K$^+$ ions. Interestingly, I230 in Kv1.2 corresponds to I287 in the *Shaker* K$^+$ channel, the mutation of which to histidine has been shown to turn the VSD into a proton pore; this residue is suggested to be part of a hydrophobic plug that
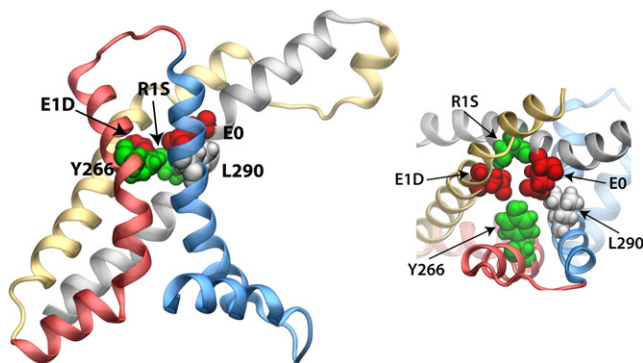

FIGURE 7 Maximum constriction region near the center of the VSD (-1 Å $< z < 6$ Å). Residues E0, E1D, R1S, L290, and Y266 are highlighted (*van der Waals representation*) and colored according to their chemical properties, namely, acidic (*red*), basic (*blue*), hydrophobic (*white*), and hydrophilic (*green*).

TABLE 2 Residues of the VSD interacting with the permeating K$^+$ ions

S1 Segment		S2 Segment		S3 Segment		S4 Segment	
Kv1.2	*Shaker*	Kv1.2	*Shaker*	Kv1.2	*Shaker*	Kv1.2	*Shaker*
V172	V236	F223	F280	Y266	No data	D280	No data
S176	S240	E1D	E283	E273	No impact	Q283	No data
S179	No data	I230	No data	E276	No impact	Q286	Q354
F180	F244	F233	F290			L290	L358
E0	E247	E236	No data			R297	R365

Residues from the VSD of the Kv1.2 channel residues identified in the simulations to interact (as defined in Fig. 5) with permeating K$^+$ ions are compared with the residues reported to be relevant for the ω-current in experimental studies of the *Shaker* channel (15).

separates the water-accessible crevices on the two sides of the VSD (14). A further comparison of the residues identified in the simulation to interact with the ions and those determined in the experiments is provided in the Supporting Material along with a discussion of the ion selectivity of the ω-pore.

Implications for the resting state conformation

The impact that various mutations have on the ω-current indirectly reflects the conformation of the VSD in the resting state. This series of simulations allow the identification of the amino acids lining the permeation pathway along the ω-pore, and show a negatively charged constriction region in the middle of the membrane that could act as a selectivity filter by providing an energetically high barrier against the permeation of anions. Two highly conserved residues, E1 and R1, are located at the constriction region and face the permeation pathway of the ions. Tombola et al. (15) have examined how a second mutation on the VSD affects the magnitude of the ω-current in the background of the R1S mutant. These measurements showed that the largest increase in the ω-current was produced by the charge-conserving E1D mutation. This observation strongly suggests that both residues, R1 and E1, must be in close proximity, in a region that represents a bottleneck for the passage of ions through the VSD.

The resting-state conformation of the VSD simulated here provides a basis to rationalize and understand such observations. In this model, E1 and R1 are located at the narrowest region of the ω-pore and a salt bridge between the two residues in the wild-type VSD seals the ω-pore. In contrast, the E1-R1 salt bridge is not present in the resting state model simulated previously by Delemotte et al. (18). The existence of an E1-R1 salt bridge in the resting state of the Kv1.2 channel is further supported by a recent study of the voltage-gated NaChBac Na$^+$ channel, which also concluded that R1 interacts primarily with the acidic residue corresponding to E1 along S2 in the resting-state conformation (40). Although the overall backbone conformation of the two simulated models share many broad features, differences in the magnitude of the vertical displacement of the S4 helix upon voltage gating are an important issue. In the resting-state model constructed by Delemotte et al. (18), the side chain R1 was forced (via energy restraints) to point toward the lower acidic residue E2 along the S2 helix, which is closer to the intracellular side of the membrane, to satisfy a putative electrostatic interaction inferred by Tao et al. (41). This resulted in a slightly lower position for the S4 helix in their model. However, a recent computational analysis demonstrated that the position of the S4 helix in our resting-state model of the VSD, in fact, is consistent with all available experimental data, including the results from Tao et al. (41); see Vargas et al. (42) for discussion.

CONCLUSION

We have employed MD simulations to investigate ion permeation through the VSD of Kv1.2 in a structural model of the resting state refined in a previous study (20). As observed in the simulation study of Delemotte et al. (18), one general impact of the mutation of the first gating arginine (R1) is to widen the pore at the center of the VSD, opening an aqueous permeation pathway that allows permeation of both K$^+$ and Cl$^-$ ions across the membrane. MD trajectories reveal the permeation pathway of the ions through aqueous crevices of the VSD. Protein residues identified to interact with the permeating ions are in excellent agreement with experimental results for the *Shaker* K$^+$ channel (15), suggesting that the resting-state structure of Kv1.2 obtained through modeling (12,13) and simulation (20) is representative of the VSD in the resting state.

The simulations reveal a narrow constriction region within the ω-pore that is lined by two highly conserved acidic residues, E0 and E1 (or E1D), and two hydrophobic side chains of L290 and Y266. Mutation of these residues has been shown to strongly affect the magnitude of the ω-current (15). The ion conduction pore narrows to ~3.5 Å in diameter near the center of the membrane, which results in a barrier against the crossing of the ions. Absence of a specific binding site for the permeating ions (in this case, cations) is consistent with the weak selectivity of the pore among different cations. At the same time, a negatively charged barrier excludes permeation of anions through the pore. Delemotte et al. (18) have also attributed cation selectivity of the ω-pore to the excess acidic residues of the VSD after neutralization of the gating arginine residues. Strong enhancement of the current upon the second mutation (E1D) both in experiment (15) and in our simulations suggest that these residues are located in a region forming a bottleneck for the permeation of ions through the VSD.

A key shortcoming of our study is the limited simulation time and, therefore, the limited conduction event statistics achieved. This is particularly unfortunate in the case of the single mutants, which display a fairly low conduction rate. The problem is partly alleviated with the simulations of the double mutants, for which a larger number of spontaneous conduction events was observed. Nevertheless, this study offers strong evidence on the mechanism and ion permeation pathway of the ω-pore. The pathway is defined through the amino acids listed in Table 2; key aspects of the conduction mechanism, in particular the geometry of the pore and existence of a narrow constriction barrier (acting as a selectivity filter) within the VSD, are extracted from single permeation trajectories and are consistent over the simulations for four mutants.

The permeation pathway of cations through the ω-pore has been suggested to overlap with the gating pores through which gating arginines are translocated during opening of the main conduction pore (15). A slight rotation and tilting

movement of the S4 segment during the gating process of the *Shaker* K$^+$ channel translates the S4 arginines along segments S1–S3 and transfers them across the membrane. In the native, nonconductive VSD, the ω-pore is always occluded by one of the arginine side chains that are engaged in strong electrostatic interactions with neighboring transmembrane helices (S1–S3) (39). These interactions are essential for stabilizing the highly charged transmembrane helices of the VSD inside the membrane and for preventing leak currents in voltage-gated cation channels known to cause periodic paralysis (43). However, in conducting mutants of VSD, the occlusion by R1 is eliminated and an ω-current does indeed arise along the space occupied by the arginine side chains.

It is interesting to pause and note the fact that the ω-pore preferably conducts cations over anions. On its face, this observation remains somewhat surprising given the numerous positively charged residues located along the S4 transmembrane helix; there are six highly conserved, positively charged residues along S4 (R1, R2, R3, R4, K5, and R6) and only four highly conserved negatively charged residues (E0, E1, E2, and D3). Yet, the VSD is predominantly cation-selective whereas its net charge is positive, and remains so even for the single mutant. This important and nontrivial qualitative feature is captured by our simulations and explained by the location of the conserved acidic residues near the hourglass-shaped pore constriction region at the center of the VSD. Enhanced conduction was observed for the double mutants E1D-R1S and E1D-R1N in the simulations, in accord with experimental data (15), which is consistent with the arginine R1 and the glutamic E1 side chains being in close proximity in the resting state (13,20,40,42). These results broadly support the overall conformation of the resting state of the VSD simulated here.

SUPPORTING MATERIAL

One table, two figures, and a detailed comparison between the results of the simulation and experiments are available at http://www.biophysj.org/biophysj/supplemental/S0006-3495(11)05349-5.

REFERENCES

1. Lee, S. Y., A. Lee, …, R. MacKinnon. 2005. Structure of the KvAP voltage-dependent K$^+$ channel and its dependence on the lipid membrane. *Proc. Natl. Acad. Sci. USA* 102:15441–15446.

2. Long, S. B., E. B. Campbell, and R. MacKinnon. 2005. Crystal structure of a mammalian voltage-dependent *Shaker* family K$^+$ channel. *Science* 309:897–903.

3. Long, S. B., X. Tao, …, R. MacKinnon. 2007. Atomic structure of a voltage-dependent K$^+$ channel in a lipid membrane-like environment. *Nature* 450:376–382.

4. Posson, D. J., P. Ge, …, P. R. Selvin. 2005. Small vertical movement of a K$^+$ channel voltage sensor measured with luminescence energy transfer. *Nature* 436:848–851.

5. Cha, A., G. E. Snyder, …, F. Bezanilla. 1999. Atomic scale movement of the voltage-sensing region in a potassium channel measured via spectroscopy. *Nature* 402:809–813.

6. Yellen, G. 1998. The moving parts of voltage-gated ion channels. *Q. Rev. Biophys.* 31:239–295.

7. Chanda, B., O. K. Asamoah, …, F. Bezanilla. 2005. Gating charge displacement in voltage-gated ion channels involves limited transmembrane movement. *Nature* 436:852–856.

8. Posson, D. J., and P. R. Selvin. 2008. Extent of voltage sensor movement during gating of *Shaker* K$^+$ channels. *Neuron* 59:98–109.

9. Murata, Y., H. Iwasaki, …, Y. Okamura. 2005. Phosphoinositide phosphatase activity coupled to an intrinsic voltage sensor. *Nature* 435:1239–1243.

10. Ramsey, I. S., M. M. Moran, …, D. E. Clapham. 2006. A voltage-gated proton-selective channel lacking the pore domain. *Nature* 440:1213–1216.

11. Sasaki, M., M. Takagi, and Y. Okamura. 2006. A voltage sensor-domain protein is a voltage-gated proton channel. *Science* 312:589–592.

12. Yarov-Yarovoy, V., D. Baker, and W. A. Catterall. 2006. Voltage sensor conformations in the open and closed states in ROSETTA structural models of K$^+$ channels. *Proc. Natl. Acad. Sci. USA* 103:7292–7297.

13. Pathak, M. M., V. Yarov-Yarovoy, …, E. Y. Isacoff. 2007. Closing in on the resting state of the *Shaker* K$^+$ channel. *Neuron* 56:124–140.

14. Campos, F. V., B. Chanda, …, F. Bezanilla. 2007. Two atomic constraints unambiguously position the S4 segment relative to S1 and S2 segments in the closed state of *Shaker* K channel. *Proc. Natl. Acad. Sci. USA* 104:7904–7909.

15. Tombola, F., M. M. Pathak, …, E. Y. Isacoff. 2007. The twisted ion-permeation pathway of a resting voltage-sensing domain. *Nature* 445:546–549.

16. Nishizawa, M., and K. Nishizawa. 2008. Molecular dynamics simulation of Kv channel voltage sensor helix in a lipid membrane with applied electric field. *Biophys. J.* 95:1729–1744.

17. Bjelkmar, P., P. S. Niemelä, …, E. Lindahl. 2009. Conformational changes and slow dynamics through microsecond polarized atomistic molecular simulation of an integral Kv1.2 ion channel. *PLOS Comput. Biol.* 5:e1000289.

18. Delemotte, L., W. Treptow, …, M. Tarek. 2010. Effect of sensor domain mutations on the properties of voltage-gated ion channels: molecular dynamics studies of the potassium channel Kv1.2. *Biophys. J.* 99:L72–L74.

19. Schow, E. V., J. A. Freites, …, D. J. Tobias. 2010. Down-state model of the voltage-sensing domain of a potassium channel. *Biophys. J.* 98:2857–2866.

20. Khalili-Araghi, F., V. Jogini, …, K. Schulten. 2010. Calculation of the gating charge for the Kv1.2 voltage-activated potassium channel. *Biophys. J.* 98:2189–2198.

21. Starace, D. M., and F. Bezanilla. 2001. Histidine scanning mutagenesis of basic residues of the S4 segment of the *Shaker* K$^+$ channel. *J. Gen. Physiol.* 117:469–490.

22. Starace, D. M., and F. Bezanilla. 2004. A proton pore in a potassium channel voltage sensor reveals a focused electric field. *Nature* 427:548–553.

23. Tombola, F., M. M. Pathak, and E. Y. Isacoff. 2005. Voltage-sensing arginines in a potassium channel permeate and occlude cation-selective pores. *Neuron* 45:379–388.

24. Gamal El-Din, T. M., H. Heldstab, …, N. G. Greeff. 2010. Double gaps along *Shaker* S4 demonstrate omega currents at three different closed states. *Channels (Austin)* 4:93–100.

25. Seoh, S. A., D. Sigg, …, F. Bezanilla. 1996. Voltage-sensing residues in the S2 and S4 segments of the *Shaker* K$^+$ channel. *Neuron* 16:1159–1167.

26. Aggarwal, S. K., and R. MacKinnon. 1996. Contribution of the S4 segment to gating charge in the *Shaker* K$^+$ channel. *Neuron* 16:1169–1177.

27. Schoppa, N. E., K. McCormack, …, F. J. Sigworth. 1992. The size of gating charge in wild-type and mutant *Shaker* potassium channels. *Science* 255:1712–1715.

28. Humphrey, W., A. Dalke, and K. Schulten. 1996. VMD: visual molecular dynamics. *J. Mol. Graph.* 14:33–38, 27–28.

29. MacKerell, Jr., A. D., D. Bashford, …, M. Karplus. 1998. All-atom empirical potential for molecular modeling and dynamics studies of proteins. *J. Phys. Chem. B* 102:3586–3616.

30. MacKerell, Jr., A. D., M. Feig, and C. L. Brooks, 3rd. 2004. Extending the treatment of backbone energetics in protein force fields: limitations of gas-phase quantum mechanics in reproducing protein conformational distributions in molecular dynamics simulations. *J. Comput. Chem.* 25:1400–1415.

31. Khalili-Araghi, F., E. Tajkhorshid, and K. Schulten. 2006. Dynamics of K$^+$ ion conduction through Kv1.2. *Biophys. J.* 91:L72–L74.

32. Jensen, M. Ø., D. W. Borhani, …, D. E. Shaw. 2010. Principles of conduction and hydrophobic gating in K$^+$ channels. *Proc. Natl. Acad. Sci. USA* 107:5833–5838.

33. Roux, B., T. W. Allen, …, W. Im. 2004. Theoretical and computational models of biological ion channels. *Q. Rev. Biophys.* 37:15–103.

34. Ahern, C. A., and R. Horn. 2005. Focused electric field across the voltage sensor of potassium channels. *Neuron* 48:25–29.

35. Ledwell, J. L., and R. W. Aldrich. 1999. Mutation in the S4 region isolates the final voltage-dependent cooperative step in potassium channel activation. *J. Gen. Physiol.* 113:384–414.

36. Lai, H. C., M. Grabe, …, L. Y. Jan. 2005. The S4 voltage sensor packs against the pore domain in the KAT1 voltage-gated potassium channel. *Neuron* 47:395–406.

37. Pathak, M., L. Kurtz, …, E. Isacoff. 2005. The cooperative voltage sensor motion that gates a potassium channel. *J. Gen. Physiol.* 125:57–69.

38. Tiwari-Woodruff, S. K., C. T. Schulteis, …, D. M. Papazian. 1997. Electrostatic interactions between transmembrane segments mediate folding of *Shaker* K$^+$ channel subunits. *Biophys. J.* 72:1489–1500.

39. Tiwari-Woodruff, S. K., M. A. Lin, …, D. M. Papazian. 2000. Voltage-dependent structural interactions in the *Shaker* K$^+$ channel. *J. Gen. Physiol.* 115:123–138.

40. DeCaen, P. G., V. Yarov-Yarovoy, …, W. A. Catterall. 2009. Sequential formation of ion pairs during activation of a sodium channel voltage sensor. *Proc. Natl. Acad. Sci. USA* 106:22498–22503.

41. Tao, X., A. Lee, …, R. MacKinnon. 2010. A gating charge transfer center in voltage sensors. *Science* 328:67–73.

42. Vargas, E., F. Bezanilla, and B. Roux. 2011. In search of a consensus model of the resting state of a voltage-sensing domain. *Neuron* 72:713–720.

43. Sokolov, S., T. Scheuer, and W. A. Catterall. 2007. Gating pore current in an inherited ion channelopathy. *Nature* 446:76–78.